Energy 249 (2022) 123639

Contents lists available at ScienceDirect

Energy

journal homepage: www.elsevier.com/locate/energy

A multi-output AC/DC energy conversion system for grid integration of bioelectrochemical power-to-gas storage

Mahdi Shahparasti [a, *], Amirhossein Rajaei [b], Andres Tarrassó [c], Alvaro Luna [c]

[a] School of Technology and Innovations, University of Vaasa, 65200, Vaasa, Finland
[b] Department of Electrical and Electronics Engineering, Shiraz University of Technology, Shiraz, 71557-13876, Iran
[c] Department of Electrical Engineering, Technical University of Catalonia, 08222, Barcelona, Spain

ARTICLE INFO

Article history:
Received 26 May 2021
Received in revised form
31 January 2022
Accepted 2 March 2022
Available online 11 March 2022

Index Terms:
AC/DC power Conversion
Bioelectrochemical energy storage (BES)
Hardware-in-the-loop (HIL)
Modular multi-level converter
Power-to-Gas
Power electronics

ABSTRACT

Bioelectrochemical Energy Storage (BES) systems are able to convert electrical power into biomethane and resemble the structure of fuel cells, as several low voltage modules are connected in series creating stacks, which are in turn parallelized to reach the desired power. However, in this case, BES modules act as gas energy storage/load that generate storable biomethane as a product. This paper proposes a multi-output multilevel AC/DC power conversion system for BES stacks. The proposed topology has a structure like a modular multi-level converter (MMC) wherein BES stacks are connected to submodules and only a capacitor exists in the DC link. Therefore, it needs only a small filter on the AC side while voltages and powers of all BES stacks are simultaneously under control. A mathematical model of the proposed power conversion system is presented, and then a control scheme has been designed in order to achieve the following goals: 1) simultaneous control of all output voltages; 2) independent control of the active and reactive power interchanged with the grid; 3) control the quality of grid current; 4) suppression of circulating current. For verification of the system performance, OPAL-RT real-time simulation results that are obtained from a 10-kW BES system containing 18 stacks are presented.

1. Introduction

To achieve the European plan in minimum 55% reduction of greenhouse gas emissions by 2030, higher shares of renewable energy and greater energy efficiency are demanded [1]. However, these resources are variable and intermittent. As a consequence, in order to keep the balance between generation and demand, producers have to either shut down power stations or pay consumers to take the extra electricity off the network. On the other hand, adding long-term and large capacity electricity storage to the power system and also sector coupling of electricity and gas sectors are promising solutions. Industrial electrochemical batteries are limited capacity energy storage systems, and they are not big enough to handle the huge level of extra power in the power system [2–4]. Other solutions such as solid oxide fuel cells (SOFCs) [5], reversible SOFC [6] and electrolyzes [7] in the range of kW to MW are currently available in the market to produce Hydrogen from electricity. However, these solutions need large tanks and infrastructures to store hydrogen. In parallel, the Power-to-Gas (P2G), especially Power-to- Methane technology, has been introduced to tackle this issue, and also to reduce system dependency on fossil fuels [8,9]. The P2G process links the power grid with the gas grid by converting a surplus of electrical power into a grid-compatible gas and there is no need for tanks to store gas [4,10].

In the last years, some BES based Power-to-Methane technologies have been proposed to convert wastewater and electricity to Methane and clean water [11,12]. A BES-based P2G can work as an energy storage system in which the excess of renewable energy production is used to feed a water depuration process for biomethane generation [13]. In this way, it is possible to accumulate energy in m^3 of methane, meanwhile, a regular industrial process of water treatment plants is conducted. Moreover, this process consumes CO_2, which contributes to reducing greenhouse emissions of this gas [14]. The use of CO_2, polluted water rich in carbon, and overproduction of renewables makes BES-based P2G a good example of the circular economy application [15].

From an electrical point of view, the BES P2G system can work as a high capacity unidirectional energy storage or in other words as a controllable AC load in microgrid and power systems [16,17].

* Corresponding author.
E-mail address: mahdi.shahparasti@uwasa.fi (M. Shahparasti).

https://doi.org/10.1016/j.energy.2022.123639
0360-5442/

Although there is still a significant gap between the current technology readiness level and a prospective large-scale BES P2G plant, chemical technology is evolving fast. It is expected that a high capacity BES P2G plant would arise shortly similar to the path of previous technologies like PV or battery that became technically and economically practical in the last decades [18]. Besides to chemical part, developing high performance and efficient AC/DC interlinking converters are vital for P2G plants grid integration.

Many BES stacks must be connected in series and parallel to make a multi-kW BES storage. They must be supplied with a controllable and consistent DC voltage. In this system, voltage balancing and equal current sharing between BES stacks are becoming more challenging to achieve [19–21]. Although the use of a diode rectifier and a DC/DC converter per stack is an easy and efficient solution to supply BES [22,23], it suffers from poor power quality on the AC side due to the nonlinearity of the diode rectifier, as well as the inability to manage reactive power and to perform grid ancillary services. In Refs. [18,24,25], a three-phase two-level voltage source converter was proposed as a solution for BES applications where many stacks were assembled in series and parallel to build a massive BES system. This solution exchanges a sinusoidal current with the grid, however, it does not guarantee a balanced distribution of voltage and consequently power among stacks. Ref. [23,26] demonstrated a galvanic isolated multi-output AC/DC topology for this application in which three-stage voltage conversions are used to build a proper interconnection between BES stacks and the grid. Although the [26]'s topology has many advantages, such as the ability to perform simultaneous control of all stacks and to draw a sinusoidal current with the desired power factor from the grid, it requires too many passive and switching components.

The MMC is an appealing and promising topology for AC/DC conversion due to its high efficiency, good harmonic performance, and modularity [27]. This topology, as an interlinking converter between the AC side with three wires and the DC side with two wires, has been utilized for various applications such as High Voltage DC transmission systems (HVDC) [28,29], Flexible AC Transmission Systems (FACTS) [30], energy storage systems [31,32] and medium voltage variable speed drives [33,34]. Widespread research has been done to address the technical challenges such as new switching methods, voltage balancing of submodules and circulating current suppression of MMC [35].

In this paper, an MMC is modified to serve as a modular multilevel multi-output (MMLMO) AC/DC converter for BES stacks, as shown in Fig. 1. In MMLMO, the BES stacks are connected to the DC side of submodules, a capacitor is mounted in the DC connection, and three grid AC grids are connected to the AC side (midpoint of each leg). With this wiring, MMLMO can control all BES stacks simultaneously. As a result, the inherent benefits of MMC have been applied to the proposed topology as follows: 1) Full controllability of BES stacks under all conditions, 2) small AC-filters, 3) Low Switching Frequency, 4) High reliability and performance, and 5) Improved scalability by the use of standardized subcomponents.

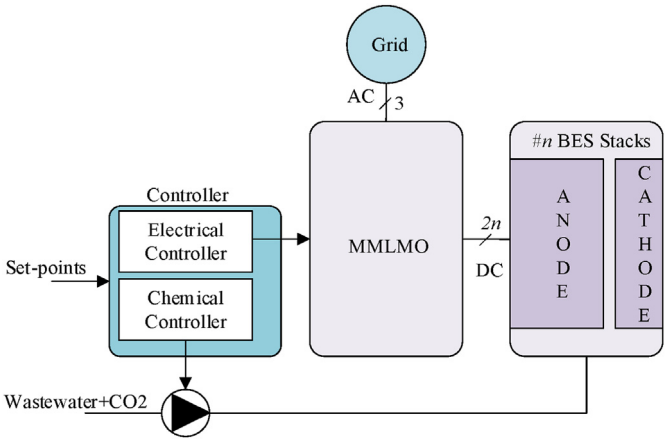

Fig. 1. Schematic of a BES system with the proposed interlinking converter.

In terms of the control scheme, the controller of the converter is responsible for 1) absorbing active power reference with desired power factor from the grid, 2) feeding all stacks with equal voltage and power. For the first goal, a three-loop power/voltage/current control scheme is developed where the DC-link voltage reference generates by the outer power loop considering the converter restrictions and grid status. Then, the middle DC-link and inner current loops are employed to determine and track the current reference, respectively. The commands of MMLMO switches are then produced using a phase-shifted pulse width modulator and a suitable sorting algorithm to provide equal and controllable voltage to all of the BES stacks.

In the following, the modelling of BES based on real data will be presented in section II. In section III, the topology of MMLMO is introduced and its equivalent circuit and mathematical model are obtained in section IV. In section V, a control scheme is suggested to accomplish the following aims: 1) simultaneous control of all outputs voltages; 2) independent exchange of active and reactive power with the grid; 3) control of the grid current power quality; 4) suppression of circulating currents between converter legs. Finally, for verification of system performance hardware in the loop system based on the OPAL-RT platform is used to validate the performance of a 10-kW BES energy storage including 18 stacks.

2. Bioelectrochemical energy storage system

BES technology is a promising solution for converting electrical power into methane [36], which is of interest at a time when the majority of energy storage systems rely on electrochemical batteries. Methane can be produced by the cathode of a BES, but its output is limited [37]. Methane production can be increased by applying a voltage to the BES cell [38].

BES cells generate methane electrochemically by reducing carbon dioxide, as shown in the chemical reaction below:

$$CO_2 + 8H^+ + 8e^- \rightarrow CH_4 + 2H_2O. \quad (1)$$

Current and voltage waveforms of the cyclic voltammetry test of a BES cell are shown in Fig. 2 [19,20]. As can be seen from these curves, the current is almost zero for voltages below E_{01}, then increases after E_{01}. Likewise, if the applied voltage exceeds the value E_{02}, the current will increase dramatically. The applied voltage should remain between E_{01} and E_{03}, otherwise, the chemical behaviour of the cell would change becoming even more unpredictable. In practice, the input voltage of BES should remain lower than1 p.u. due to isolation issues. To protect the cell, a diode can be installed in parallel [20].

So far, several electrical models have been proposed based on a resistor, a capacitor and a DC source for emulating BES and systems [41,42]. This paper aims to present a simple model to emulate the BES system in linear and nonlinear operation areas. Based on the current profile of the BES cell in Fig. 2, two lines can be used to model cell behaviour. Following this idea, the proposed model is made by two parallel R-E branches in Fig. 3, in which each line can be emulated by an electrical branch. It is worth mentioning that the diode in branch 2 is used to prevent the flow of current between branches.

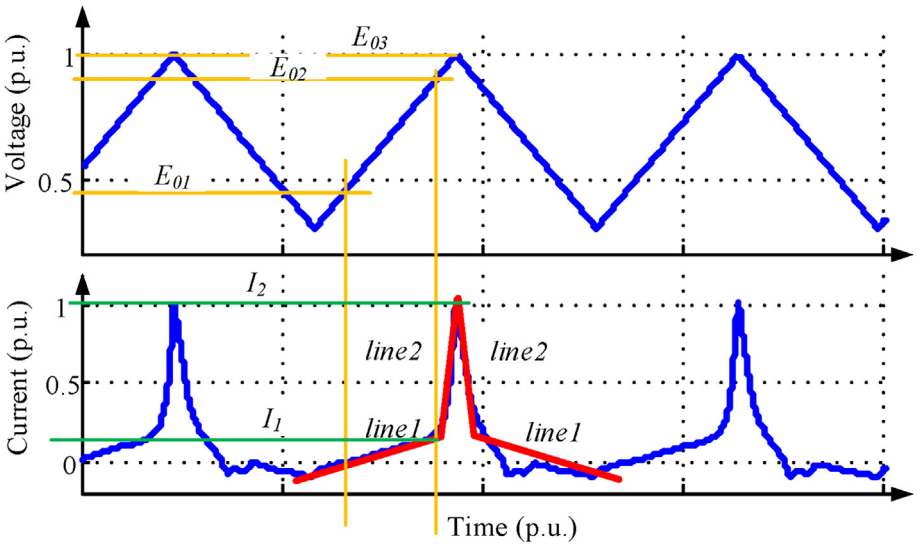

Fig. 2. The current-voltage curve for a BES cell.

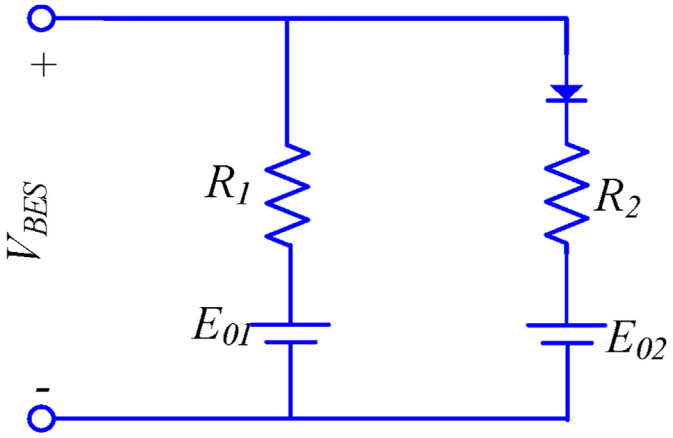

Fig. 3. A static model of the BES cell.

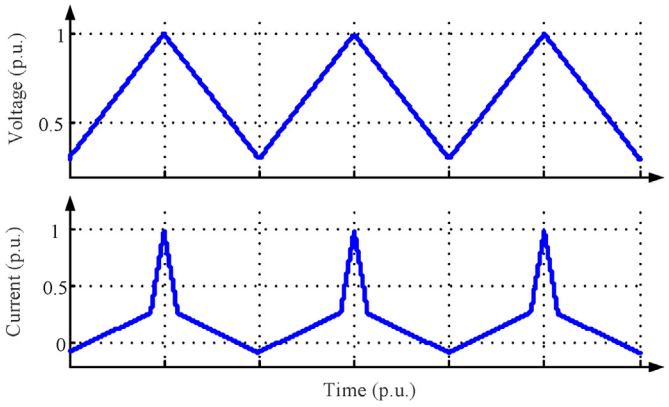

Fig. 4. Methane-Voltage and Current-Voltage curves for the proposed static model of the BES cell.

The equivalent resistances in the BES model can be found operating the following equations:

$$R_1 = \frac{E_{02} - E_{01}}{I_1}, \tag{2}$$

$$R_2 = \frac{E_{03} - E_{02}}{I_2 - \frac{E_{03}-E_{01}}{E_{02}-E_{01}} I_1}, \tag{3}$$

where values of I_1, I_2, E_{01}, E_{02}, and E_{03} can be found from the real Current-Voltage curve of the BES cell according to Fig. 2.

In order to validate this simplified model, its response is compared with the real BES response. The obtained results from the proposed model are shown in Fig. 4 which are similar to real data in Fig. 2.

Lots of BES cells have to be installed in series and parallel inside of one BES stack. Then, several BES stacks build the BES plant. For a stack, the parameters of the model can be considered as:

$$E_{01\_stack} = N_s E_{01}, \tag{4}$$

$$E_{02\_stack} = N_s E_{02}, \tag{5}$$

$$R_{1\_stack} = \frac{N_s}{N_p} R_1, \tag{6}$$

$$R_{2\_stack} = \frac{N_s}{N_p} R_2, \tag{7}$$

where N_s and N_p refer to the number of BES cells in series in one branch and the number of BES branches in parallel in the stack, respectively.

Modelling of chemical part especially methane is not possible since the measurable methane production rate is slow and variable in time, and any significant difference can be seen only with long sampling times like a week.

3. Modular multi-level multi-output AC/DC

3.1. Topology

Fig. 5 shows the electrical circuit diagram of the proposed topology (MMLMO), where six arms with a series connection of

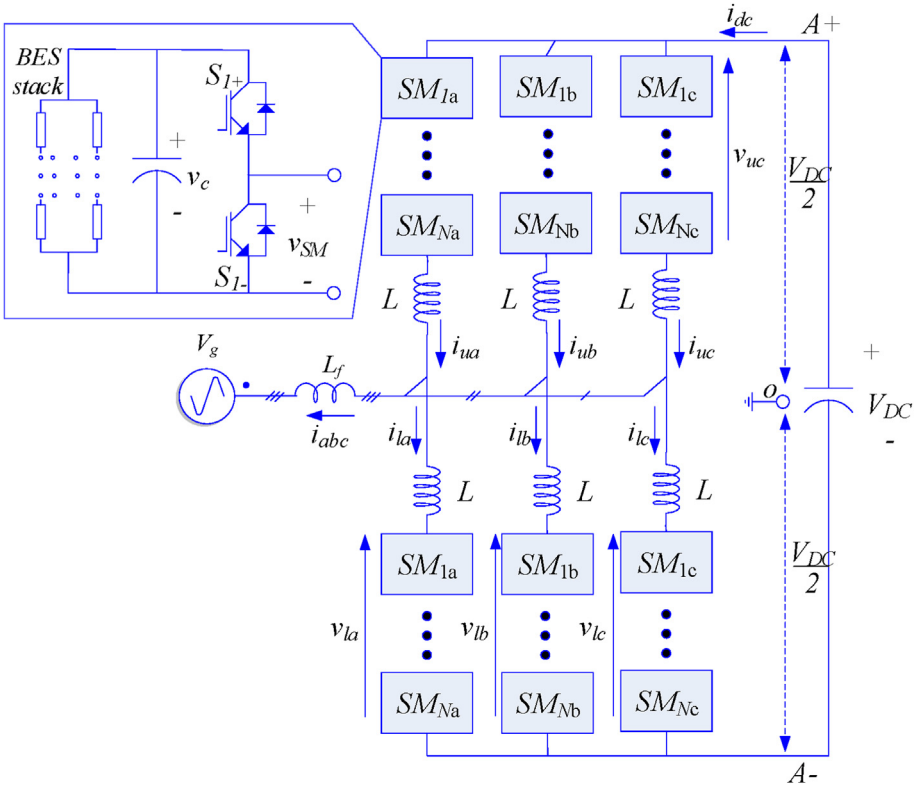

Fig. 5. Proposed Modular Multi-level Multi-output AC/DC Converter for BES stacks.

submodules are utilized to build a three-phase multi-output AC-DC converter. This converter resembles the conventional MMC with a few modifications: (1) the AC side of the converter is connected to the grid through an inductor as a low pass filter; (2) there is only one capacitor in the DC side of the converter and nothing connects to terminal *A*+ and *A*-, as shown in Fig. 5; (3) the output of each submodule connects to one BES stack. Therefore, the power absorbed from the grid transfers to BES stacks by MMLMO submodules, which produce methane and clean water.

Similar to other multilevel converters, the MMLMO can make a semi-sinusoidal AC voltage because of the series connection of several modules in each ram. Furthermore, the power factor of the grid current is simply under control.

3.2. Equivalent circuit and mathematical model

As shown in the electrical circuit diagram in Fig. 5, the proposed topology consists of six arms, and each arm has *N* submodules in series with one inductor "*L*". This inductor, *L*, is used to limit circulating and fault currents. The MMLMO consists of two arms per phase-leg, i.e., an upper arm (represented by the superscript "*u*") and a lower arm (represented by superscript "*l*"). The output terminal/midpoint of each phase leg is connected to the grid via a first-order low pass filter L_f.

Each submodule consists of a half-bridge cell that connects to one BES stack on its DC side. The output voltage of each submodule in the DC side is either equal to V_{DC}/N or open circuit depending on the switching states of the submodules switches S_{m+} and S_{m-}.

To explore the operation of the MMLMO, only one leg of the MMLMO is considered. In Fig. 5, the point "o", the fictitious DC-side mid-point, is used as a reference point. In the mathematical analysis, the point "o" is considered as the DC mid-point between the upper and lower arm which is connected to the grid.

In Fig. 5, exactly *N* modules are in the on mode and *N* modules are in the off mode in each leg at any moment. The on mode means switches S_{j+} = on, S_{j-} = off, also the off mode means inverse.

In general, the electrical behaviour of each leg can be expressed in terms of voltages and currents of upper and lower arms by the following expressions:

$$v_{uj} + v_{lj} + L\left(\frac{di_{uj}}{dt} + \frac{di_{lj}}{dt}\right) = V_{dc},\ j = a, b, c \tag{8}$$

$$i_{uj} = i_{cirj} + \frac{i_j}{2}, \tag{9}$$

$$i_{lj} = i_{cirj} - \frac{i_j}{2}, \tag{10}$$

where v_{uj} and v_{lj} are the equivalent voltages of submodules in on mode in the upper and lower arms, respectively, i_{uj} and i_{lj} are the upper and lower arm currents and i_{cirj} is the circulating current in the phase-leg *j*. The circulating current flows within three legs of the converter and thus, $i_{cira} + i_{cirb} + i_{circ} = 0$ if all legs are properly balanced. The waveform (the value) of i_{cir} does not have any effect on the DC-or/AC-side current, but it has a significant impact on the switches and the capacitors inside of each submodule. According to previous investigations, the circulating current consists of a DC component "I_{DC}" and even harmonics "I_k" [43]:

$$i_{cirj} = I_{DC} + \sum_{k=2,4,6\ldots} I_k \sin(k\omega t + \varphi_k), \tag{11}$$

$$\langle i_{cirj} \rangle = I_{DC} = i_{DC}/3, \tag{12}$$

where *k* is a positive even integer, and I_{DC} is DC-link current. Since

nothing connects between the A+ and A-terminals of the DC bus, the value of the DC-link current is zero. Thus, the DC component of the circulating current must ideally be around zero.

By writing KVL for one leg, the following relationships can be found:

$$V_{pccj} = \left(L + L_f\right)\frac{di_j}{dt} + \underbrace{\frac{v_{uj} - v_{lj}}{2}}_{E_{comj}}, \tag{13}$$

$$\left(L + L_f\right)\frac{di_{cirj}}{dt} = \frac{V_{dc}}{2} - \underbrace{\frac{v_{uj} + v_{lj}}{2}}_{E_{difj}}, \tag{14}$$

where E_{dif} represents the voltage difference between the equivalent upper and lower voltage arms, and E_{com} denotes the inner electromotive force (EMF) voltage that is controlled for exchanging power with the grid.

The AC side of MMLMO is modelled in Fig. 6 based on (13) and (14). The DC bus voltage is equal to the total voltages of the capacitors of the modules that are in the on state. Therefore, $0.5Nv_c$ is used as $V_{DC}/2$ in Fig. 6. To model the DC side of submodules, a dependent current source "i_{SMj}" is proposed as follows:

$$i_{SMj} = i_{cirj} + \frac{P_{ac} - P_{loss}}{6N}, \tag{15}$$

$$P_{ac} = v_{pcca}.i_a + v_{pccb}.i_b + v_{pccc}.i_c, \tag{16}$$

where P_{loss} and P_{ac} refer to the loss of converter and instantaneous power exchanged between the converter and the grid, respectively.

4. Proposed control scheme

In this section, a control scheme will be developed for a BES system controlled by MMLMO. The controller of the converter consists of three main sections: power, circulating current suppression and the BES stack voltage controllers. The power control is developed based on the cascade power/voltage/current loops concept and produces the voltage references for the BES stack voltage control section. These references are sent to the Pulse-width modulation (PWM) modulator to generate the pulses for the switches within the submodules. The modulation technique is established on the carrier disposition strategy that uses N triangular carriers with the same frequency and amplitude but with a phase shift of $360°/N$. This control scheme is designed such that

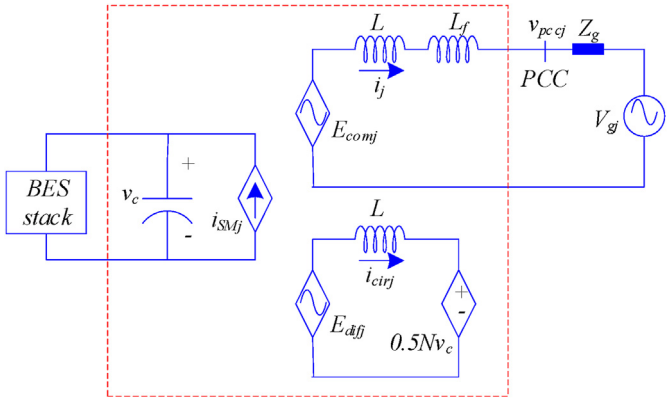

Fig. 6. Mathematical representation of the proposed converter, j = a, b, c.

firstly the DC bus voltage distributes equally between BES stacks in steady-state and transient situations. Secondly, a sinusoidal current is exchanged with the grid.

4.1. Power controller

For power controller development, it is assumed that the upper-level operator sends active and reactive power setpoints to the BES system (P^* and Q^*). Then, P^* and Q^* are tracked using a multi-loop control scheme as shown in Fig. 7. Park transformations are not required since the controller is implemented in the stationary reference frame. As a consequence, it is simpler and more effective from the computational burden point of view.

The reference of DC bus voltage V_{DC}^* is compared with its real value V_{DC}, and then the voltage error will pass through a Proportional Integral (PI) controller. The output of the PI controller equals the required active power reference by the converter ($\widehat{P}$) to fix the DC link voltage. In order to exchange a current with unity power factor with the grid, the reference of reactive power Q^* is considered zero in this paper; however, it can be set to any desired value within the converter power rating. The reference of converter current in the stationary reference frame $i_{\alpha\beta}^*$ is generated by the following expression based on $\widehat{P}$ and Q^*:

$$\begin{bmatrix} i_{\alpha+}^* \\ i_{\beta+}^* \end{bmatrix} = \frac{1.5}{v_{\alpha1+}^2 + v_{\beta1+}^2}\begin{bmatrix} v_{\alpha1+} & v_{\beta1+} \\ v_{\beta1+} & -v_{\alpha1+} \end{bmatrix}\begin{bmatrix} \widehat{P} \\ Q^* \end{bmatrix} = T^+\begin{bmatrix} \widehat{P} \\ Q^* \end{bmatrix}, \tag{17}$$

where $v_{\alpha\beta1}$ are the fundamental components of the grid voltage and the subscript + shows the positive sequence. The Dual Second Order Generalized Integrator Frequency Locked Loop (DSOGI-FLL) is used for estimating the magnitude of the symmetrical components of the voltage at the PCC [44]. To track current reference with zero steady-state error and fast dynamic response, the proportional resonant (PR) controller is utilized, which can be expressed as:

$$PR = K_p + \sum_{i=1,5,7}\frac{2\omega_c K_i s}{s^2 + 2\omega_c s + i^2\omega_o^2}, \tag{18}$$

where K_p, K_i, ω_o, and ω_c are the proportional gain, the resonant gain, the resonant frequency, and the resonant bandwidth, respectively. The tuning procedure of the PR controller parameters of a grid-connected converter was already described in Ref. [45]. The output of the power loop is E_{com} which leads to the exchanging of active and reactive powers with the grid according to (13).

4.2. Circulating current suppression controller

Following the analysis in section II, the circulation circuit in the steady-state has to be zero without any DC and AC components. Therefore, a control scheme based on PR controller at even harmonics is proposed to suppress i_{cir} as shown in Fig. 7. This controller can be described as follows:

$$PR_{cir} = K_{pcir} + \sum_{i=2,4,6,8}\frac{2\omega_{cciri} K_{icir} s}{s^2 + 2\omega_{cciri} s + i^2\omega_o^2}, \tag{19}$$

where K_{pcir}, K_{icir}, and ω_{cciri} are the proportional gain, the resonant gain, and the resonant bandwidth, respectively. Opposite of controller suggested in Refs. [43,46,47] where the only resonant controller was employed, here proportional controller is added to the resonant controller because the DC-link current must be zero in this application. Also, the bandwidth of the resonant controller is selected wide enough to reduce its sensitivity and to improve

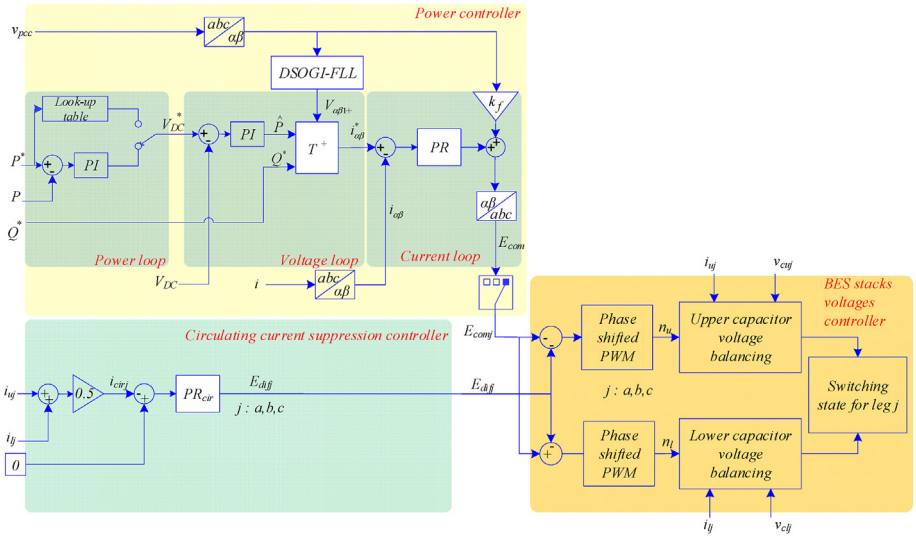

Fig. 7. The proposed control scheme to manage the output DC voltage and the input AC current.

robustness to frequency variations. The output of this part can be considered E_{dif} in (14).

4.3. BES stacks voltages controller

Finally, the outputs of power and circulating current controllers (E_{com} *and* E_{dif}) are sent to the PWM and BES stacks voltages controlling stage as shown in Fig. 7. In this paper, phase-shifted PWM is used for the switching of the converter.

For a converter with N submodules in each arm, the reference voltages are compared with N triangular carriers in which the phase angle between adjacent carrier signals is 360°/N. Then, the required number of submodules in upper/lower arms N_u/N_l are determined based on these comparisons. As it is shown in Fig. 7, the value of N_u/N_l, the voltages of BES stacks (capacitors of submodules) and arms currents enter to voltage balancing block, then the switching state of each arm goes out from this block.

5. Real-time HIL simulation results

5.1. Results

In order to test the performance of the proposed multi-output AC/DC topology for power to biomethane application, an OPAL-RT OP4510 real-time simulator (see Fig. 8) has been used for real-time emulation of the system including the proposed converter, 18 BES stacks and the three-phase grid. A loopback between inputs and outputs in analogue and digital ports is utilized to realize the real system. Because of OPAL-RT limitation, MMLMO with three submodules in each arm is built inside its FPGA and the controller part is implemented in its CPU. With this structure, 18 BES stacks are fed individually and simultaneously with MMLMO.

The hardware parameters and control scheme parameters are listed also in Table 1 and Table 2. The switching frequency of the converter is set to 2 kHz because of the limited sample time of the CPU in OPAL. Also, the values of R_1, $R2$, E_1, and E_2 are set at 1.2756 kΩ, 51.9333Ω, 0 V and 295.2 V, respectively in the BES stack model. The current controller parameters (K_p, K_i, and k_f) is tuned according to the procedure described in Ref. [48].

In the first simulation, the reference of active power changes from 0 to 10 kW and inverse. The obtained results are shown in Fig. 9, in which the voltage at the PCC does not change during

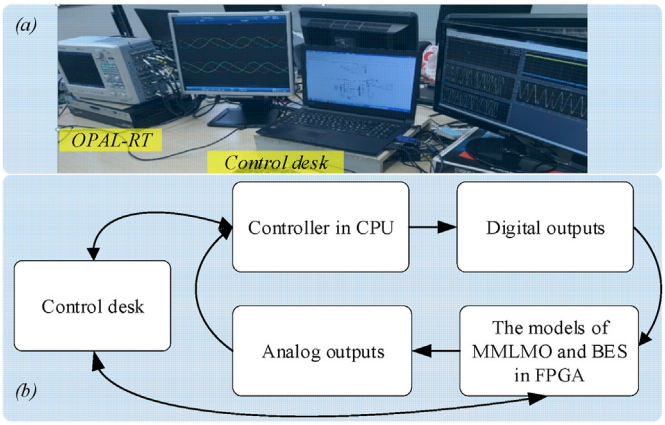

Fig. 8. The HIL setup for performing the real-time simulation.

Table 1
Proposed AC/DC converter parameters.

Parameter	Value
Grid voltage	380 V-50 Hz
Grid short circuit capacity (SCC)	15 kA
Number of submodules per Arm	3
Interface filter inductor (L_f)	3 mH
Carrier frequency	2 kHz
DC link capacitor	2200 μF
Submodules capacitors (C)	2200 μF
Arm inductor (L)	200 μH

transient and is almost fixed. The injected current to the grid varies based on its reference with a suitable performance in steady and transient states. The instantaneous value of the DC link voltage matches its reference in all moments and changes from 700 V to 1085 V. It is evident from the measured active and reactive power with the grid in Fig. 9 that the reactive power is always zero and the active power alters between zero and 10 kW. The voltages of BES stacks follow equally the reference and they remain at the same value during all the tests.

The reference and measured currents in the stationary reference frame are compared in Fig. 10 wherein the current tracking errors

Table 2
Controllers parameters.

Controller	Parameters
Dc link Voltage Controller	$K_p = 0.3$, $K_i = 1$
Current Controller	$K_p = 0.8$, $K_i = 100$, $\omega_c = 2$
Circulation Current Controller	$K_{pcir} = 0.05$, $K_{icir2} = K_{icir4} = 1.5$, $K_{icir6} = K_{icir8} = 1$, $\omega_{ccir} = 2$ rad/s

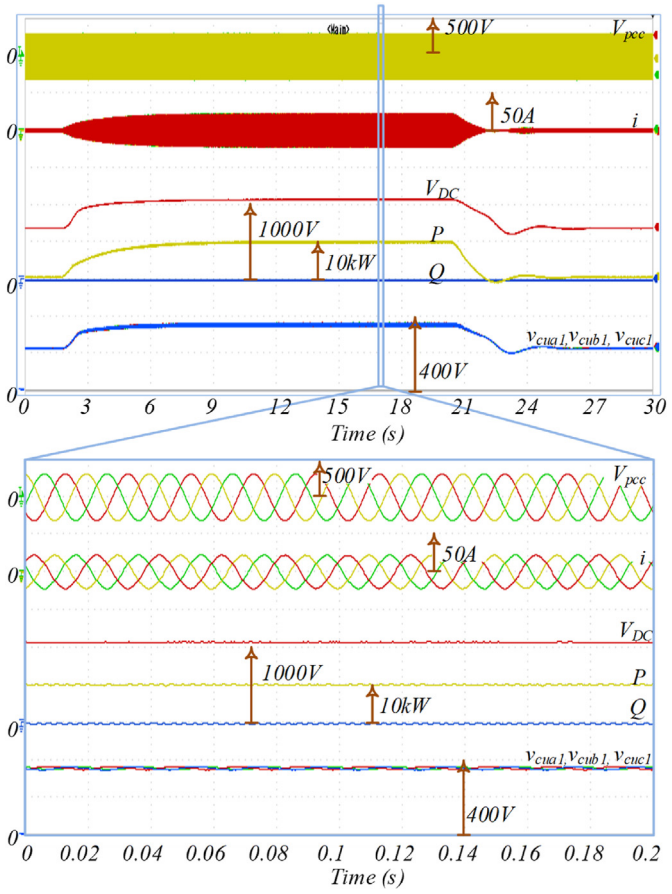

Fig. 9. Active power reference step change from 0 to 10 kW and inverse. From top: grid voltage (V_{pcc}), grid current (i, 50A/div), DC link voltage (V_{DC}), active power (P), reactive power (Q), submodules voltages (v_c).

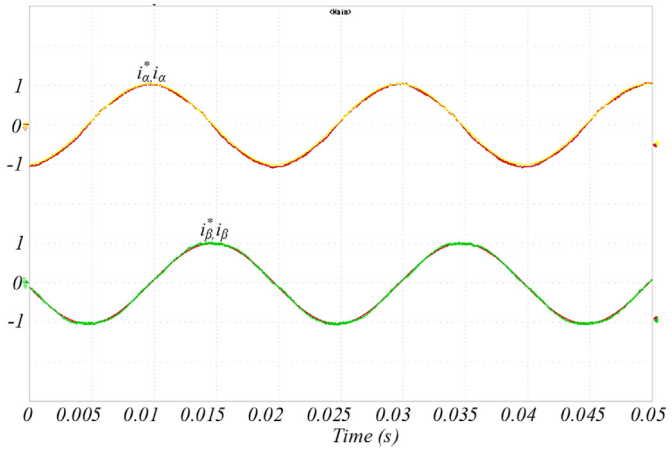

Fig. 10. Proof of current reference tracking: actual and reference currents (in p.u.).

are around zero for both axes. In turn, Fig. 11 depicts the applied voltages to the BES stacks in the steady-state. The voltage ripple shown is around 5% which is an acceptable percentage for BES stacks as they have a very slow dynamic response.

In the second scenario, as shown in Fig. 12, the active power reference changes from 0 kW to 2 kW first, then changes from 2 kW to 10 kW. The achieved results reveal that the active power absorbed from the network is not proportional to the DC voltage due to the nonlinear characteristic of BES. Changing the DC voltage from 700 V to 910 V (200 V), for example, results in an active power change of about 2 kW. However, 175 V is needed for an 8 kW active power step change when the DC voltage is 910 V.

The performance of the proposed circulating current controller is also evaluated in this section. This controller has proportional and resonant parts. The obtained results in Fig. 13 show the effect of activating each part of this controller. In the first part of the test, the arms currents have even harmonics and the peak value is around 40 A. In the next part, the current peaks are reduced due to the activation of the proportional part of the controller. Then, the shape of the currents become almost sinusoidal with adding resonant controller in even harmonics in the last part of the test. In the end, the value of the circulating current ($0.5i_{ua} + 0.5i_{la}$) is reduced to zero.

The AC components of the voltages applied to BES stacks (submodules voltages) without and with the circulating current controller are shown in Fig. 14 and Fig. 15, respectively. It is clear that the even harmonics are removed from the voltages of the capacitors with the proposed controller, but the peak to peaks of voltages ripples do not change a lot and they are almost the same.

5.2. Discussion and comparison

1. The principle operation of MMLMO can be quickly deduced from the results presented above. MMLMO allows feeding each BES module individually while exchanging active and reactive power independently with the grid. A balanced and sinusoidal current flow at the AC side of the MMLMO side while desired power factor is maintained.
2. The above simulation results show the MMLMO behaviour seen from both AC- and DC-side terminals for the step-up and step-down of power reference. Figs. 9 and 12 show the waveforms of grid voltage, grid current, DC link voltage, active and reactive powers, as well voltages of upper arm SM capacitors. There is a common pattern to all of these responses:
   - Active and reactive powers are fully under control, and other variables are changed accordingly. The powers were changed with a smooth and controlled transient response and their steady-state errors are around zero. In the simulations, the reactive power setpoint is set to zero, but it can be set to any desired value.
   - DC link and output DC voltages are changed depending on the reference of active and reactive power. They exhibit acceptable transient and steady-state responses.
   - Voltage ripples of the output DC voltages are also very small and they are within a 5% margin in all cases. Moreover, the

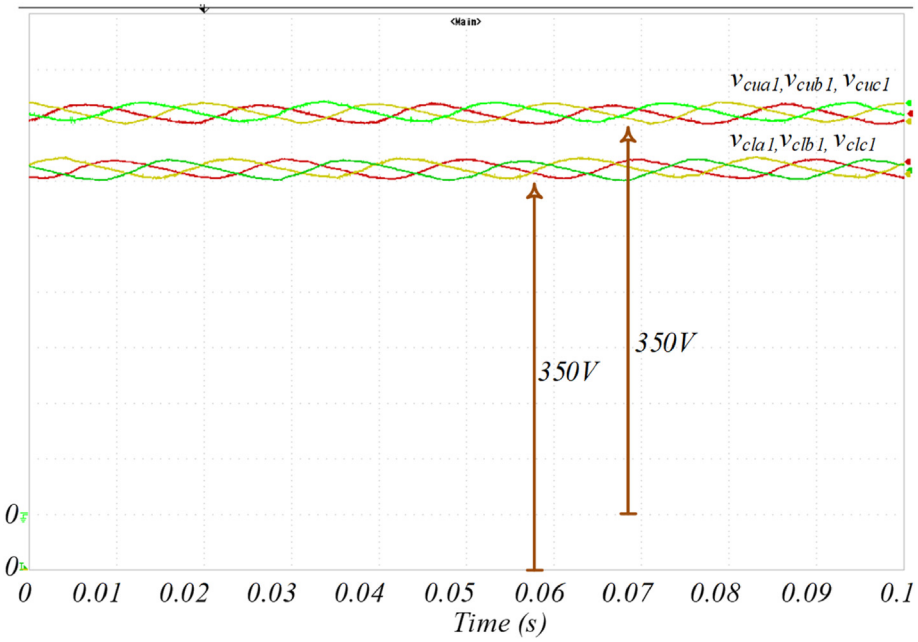

Fig. 11. Applied voltages to BES stacks in steady-state, submodules voltages, (v_c).

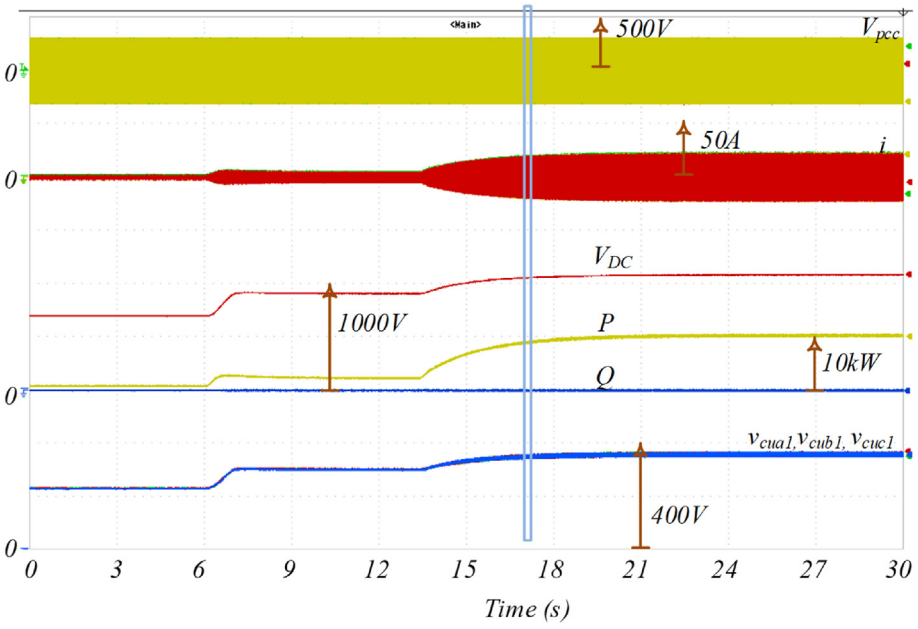

Fig. 12. Active power reference step change from 0 to 2 kW and then 10 kW. From top: grid voltage (V_{abc}), grid current (i_{abc}), DC link voltage (V_{DC}), active power (P), reactive power (Q), submodules voltages (v_c).

difference among output voltages even different MMLMO phases are also very slight and they are less than 1% margin.
- Grid current is AC and sinusoidal and does not have any DC offset. The overshoot phenomenon is not observed in the current response.

3. Another important aspect to be considered is the circulating current in MMLMO. In MMLMO, as shown in Figs. 13–15, the circulating current is fully under control thanks to the proposed control scheme which has a positive impact on waveforms of arm current. Simulation results confirm that the arms currents become sinusoidal without any distortion with this controller.
4. As a default assumption, a low harmonic distortion can be gained at the AC side of MMLMO due to having inherent advantages of modular multi-level converters. By combining this configuration with a phase-shifted PWM modulation technique, a quasi-sinusoidal voltage waveform with a low harmonic distortion can be produced. Therefore, instead of using high order low phase filters such as LCL filter at AC side, a small size first order L filter is used in this paper. This simple L filter is adequate to reach current waveforms with low harmonic distortion. Each output DC stage is only included a capacitor

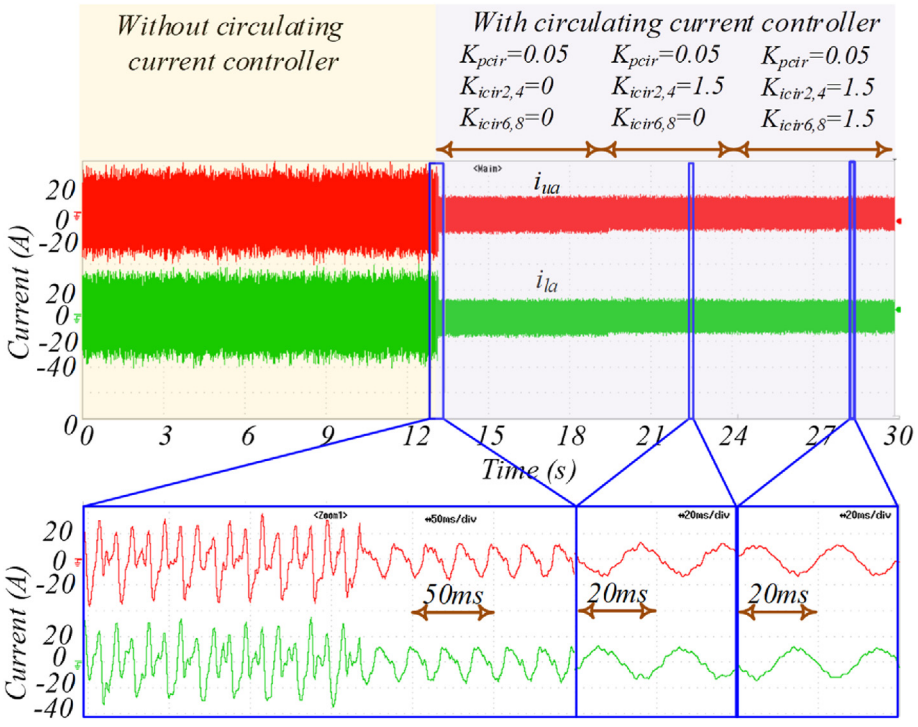

Fig. 13. Proof of the efficiency of the proposed circulating controller: Current of upper and lower arms in phase *a* (i_{ua},i_{la},).

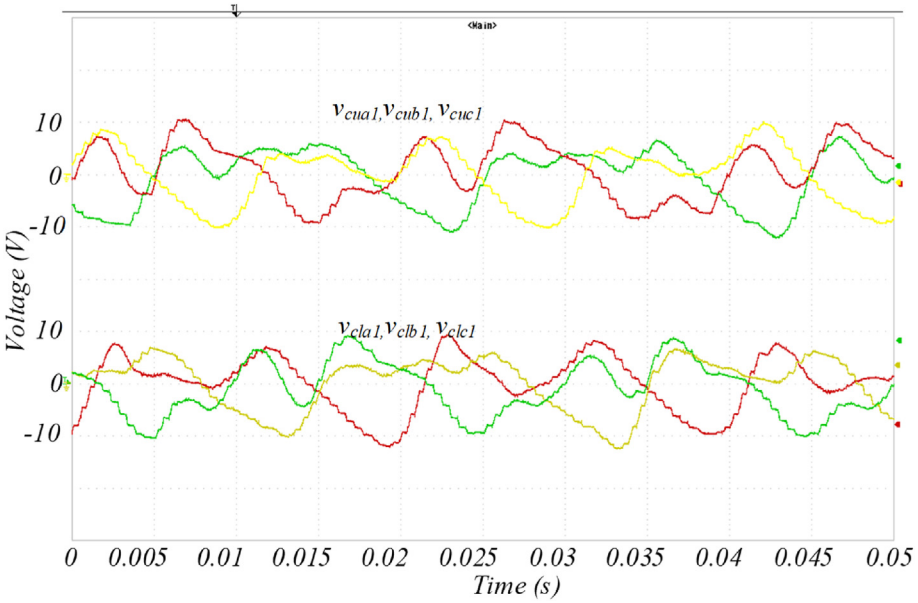

Fig. 14. Proof of the efficiency of the proposed circulating controller: AC component of BES stacks voltages without circulating current controller (v_c).

which must be selected big enough to reduce the DC voltage ripple.

5. Last but not least, the MMLMO design involves both AC and DC sides filters. There is a close connection between the power rating, the number of submodules, switching methods in MMLMO. Future work should furthermore be addressed to an optimum design of filters in terms of order and sizing to be installed at both AC and DC sides of the MMLMO. It can be predicted that adding a dc/dc converter at the output of each submodule is possible to reduce the submodule capacitor size and reduce the output DC voltage ripple.

A comparison between the proposed MMLMO power conversion system and other BES power converters is done in Table 3. It can be seen that MMLMO is the best in terms of the numbers of semiconductors and passive components and also electrical behaviours in AC and DC sides. No galvanic isolation can be mentioned as a weakness for MMLMO, however, it is not mandatory in many cases.

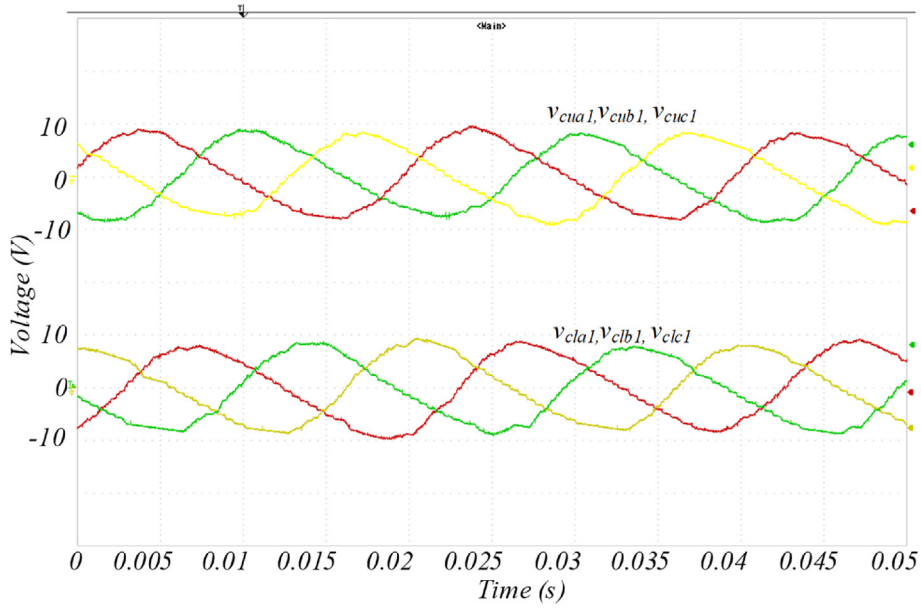

Fig. 15. Proof of the efficiency of the proposed circulating controller: AC component of BES stacks voltages with circulating current controller (v_c).

Table 3
Comparison of power converters for BES systems.

Ref	AC side	DC side	Number of switches	Number of diodes	Passive components	Advantages	Disadvantages
[18,25]	Two-level pulsed voltage	No individual supply	6 in total	6 in total	LCL filter on AC side, and C on DC side	- Cheap - No need for many passive components and semiconductors	- Unable to feed BES steaks individually - Low reliability - Unequal voltage sharing - No Galvanic isolation.
[23]-**Topology 1 in Fig. 1**	Two-level pulsed voltage	Individual supply	6 in AC side and 4 per output	4 per output	Transformer + LC filters in AC and DC sides	- Galvanic isolation	- This needs many semiconductors. - Complexity of control scheme.
[23]-**Topology 2 in Fig. 2**	Two-level pulsed voltage	Individual supply	6 in AC side and 4 per output	4 per output	- Only an LC filter in AC and a C filter on the DC side	- There is a possibility to add a battery to the system	- This needs many semiconductors. - Complexity of control scheme. - No galvanic isolation
[26]	Two-level pulsed voltage	Individual supply	6 in AC side and 1 per output	5 per output	Transformer + LC filters in AC and DC sides	- Galvanic isolation. - Unified and sample control scheme	- This needs many semiconductors.
Proposed	Semi-sinusoidal	Individual supply	2 per output	2 per output	Only an L filter in AC and a C filter on the DC side	- Minimum number of passive components and semiconductors - Unified control scheme	- No galvanic isolation

6. Conclusion

A single-stage/multi-output AC/DC topology was established on the modular multilevel converter concept, which is suitable to be employed as an interface for power to biomethane application. This topology only requires two switches and one capacitor per output DC voltage. Up to the knowledge of authors, this is the lowest number of elements compared to available BES power converters. First, the mathematical models and equivalent circuit diagrams of BES cell and the proposed topology were developed; next, a comprehensive control scheme was designed by considering the following constraints 1) feeding the output loads, 2) the internal limitations of the converter, 3) the suppression of circulating current, and 4) the control of the power and current exchanged with the grid. OPAL-RT OP4510 Real-time simulator was used for validation. The FPGA and CPU of OP4510 were programmed to model the hardware and to implement the controller, respectively. The real-time results of a 10 kW BES system with 18 BES stacks confirmed that this topology is a high potential solution to feed BES stacks individually, to control active and reactive power, and to mitigate the AC circulating current simultaneously. Results demonstrated that the active and reactive powers are independently tracked the references without over/undershoots, and the steady-state error is negligible. Although a simple L filter is used on the AC side, the current is sinusoidal because of its multilevel feature. Voltages across BES stacks deduced that they are fed individually with equal voltage simultaneously in all cases wherein their voltage ripples are within a 5% margin, as well as the difference among output voltages are less than 1% margin.

Future work can be done to obtain a more practical realization of MMLMO based on available semiconductors in the market, optimum operating point and efficiency. A more precise representation

of semiconductor losses will produce more realistic results of the MMLMO efficiency and will provide hints for new control methods to upgrade the efficiency. This improved representation can furthermore provide some tips on the switching frequencies and strategies that are applicable to control MMLMO.

Credit author statement

Mahdi Shahparasti: Conceptualization, Methodology, Software, Validation, Writing – original draft. Amirhossein Rajaei: Reviewing and Editing. Andrés Tarrassó; : Validation. Alvaro Luna: Reviewing and Editing, Project administration.

Declaration of competing interest

The authors declare that they have no known competing financial interests or personal relationships that could have appeared to influence the work reported in this paper.

Acknowledgements

The research leading to these results has received funding from the European Union's Horizon 2020 research and innovation programme under the Marie Skłodowska-Curie grant agreement No 712949 (TECNIOspring PLUS) and from the Agency for Business Competitiveness of the Government of Catalonia. Also, this work has been supported by the Spanish Ministry of Economy and Competitiveness under the projects RTI2018-100921-B- C21. Any opinions, findings and conclusions or recommendations expressed in this material are those of the authors and do not necessarily reflect those of the host institutions or funders.

References

[1] Delivering the European green deal. European Commission; 2021. https://ec.europa.eu/info/strategy/priorities-2019-2024/european-green-deal/delivering-european-green-deal_en. [Accessed 9 January 2022].
[2] Yan L, Peng J, Gao D, Wu Y, Liu Y, Li H, et al. A hybrid method with cascaded structure for early-stage remaining useful life prediction of lithium-ion battery. Energy 2021;243:123038. https://doi.org/10.1016/j.energy.2021.123038.
[3] Shi J, Xu B, Shen Y, Wu J. Energy management strategy for battery/supercapacitor hybrid electric city bus based on driving pattern recognition. Energy 2021:122752. https://doi.org/10.1016/j.energy.2021.122752.
[4] Zhang D, Zhu H, Zhang H, Goh HH, Liu H, Wu T. An optimized design of residential integrated energy system considering the power-to-gas technology with multi-functional characteristics. Energy 2022;238:121774. https://doi.org/10.1016/j.energy.2021.121774.
[5] Vitale F, Rispoli N, Sorrentino M, Rosen MA, Pianese C. On the use of dynamic programming for optimal energy management of grid-connected reversible solid oxide cell-based renewable microgrids. Energy 2021;225:120304. https://doi.org/10.1016/j.energy.2021.120304.
[6] Mayyas A, Chadly A, Amer ST, Azar E. Economics of the Li-ion batteries and reversible fuel cells as energy storage systems when coupled with dynamic electricity pricing schemes. Energy 2022;239:121941. https://doi.org/10.1016/j.energy.2021.121941.
[7] Giap VT, Lee YD, Kim YS, Bui T, Ahn KY. New definition of levelized cost of energy storage and its application to reversible solid oxide fuel-cell. Energy 2022;239. https://doi.org/10.1016/j.energy.2021.122220.
[8] ElMekawy A, Hegab HM, Mohanakrishna G, Elbaz AF, Bulut M, Pant D. Technological advances in CO2 conversion electro-biorefinery: a step toward commercialization. Bioresour Technol 2016;215:357–70. https://doi.org/10.1016/j.biortech.2016.03.023.
[9] Salehi J, Namvar A, Gazijahani FS, Shafie-khah M, Catalão JPS. Effect of power-to-gas technology in energy hub optimal operation and gas network congestion reduction. Energy 2022;240:122835. https://doi.org/10.1016/j.energy.2021.122835.
[10] Pursiheimo E, Holttinen HH, Koljonen T. Path towards 100 % renewable energy future and feasibility of power-to-gas technology in Nordic Countries. IET Renew Power Gener 2017;11:1695–706. https://doi.org/10.1049/iet-rpg.2017.0021.
[11] Kumar G, Saratale RG, Kadier A, Sivagurunathan P, Zhen G, Kim SH, et al. A review on bio-electrochemical systems (BESs) for the syngas and value added biochemicals production. Chemosphere 2017;177:84–92. https://doi.org/10.1016/j.chemosphere.2017.02.135.
[12] Jadhav DA, Ghosh Ray S, Ghangrekar MM. Third generation in bio-electrochemical system research – a systematic review on mechanisms for recovery of valuable by-products from wastewater. Renew Sustain Energy Rev 2017;76:1022–31. https://doi.org/10.1016/j.rser.2017.03.096.
[13] Karamanev D, Pupkevich V, Penev K, Glibin V, Gohil J, Vajihinejad V. Biological conversion of hydrogen to electricity for energy storage. Energy 2017;129:237–45. https://doi.org/10.1016/j.energy.2017.04.110.
[14] Guelpa E, Bischi A, Verda V, Chertkov M, Lund H. Towards future infrastructures for sustainable multi-energy systems: a review. Energy 2019;184:2–21. https://doi.org/10.1016/j.energy.2019.05.057.
[15] Ma Y, Wang H, Hong F, Yang J, Chen Z, Cui H, et al. Modeling and optimization of combined heat and power with power-to-gas and carbon capture system in integrated energy system. Energy 2021;236:121392. https://doi.org/10.1016/j.energy.2021.121392.
[16] He C, Wu L, Liu T, Bie Zhaohong, Bie Z. Robust Co-optimization planning of interdependent electricity and natural gas systems with a joint N-1 and probabilistic reliability criterion. IEEE Trans Power Syst 2017;33:2140–54. https://doi.org/10.1109/TPWRS.2017.2727859.
[17] Shahparasti M, Rajaei A, Tarraso A, Romay JDVL, Luna A. Control and validation of a reinforced power conversion system for upcoming bio-electrochemical power to gas stations. Electron 2021;10. https://doi.org/10.3390/electronics10121470.
[18] Muñoz-Aguilar RS, Molognoni D, Bosch-Jimenez P, Borràs E, Pirriera M Della, Luna Á. Design, operation, modeling and grid integration of power-to-gas bioelectrochemical systems. Energies 2018;11:1–15. https://doi.org/10.3390/en11081947.
[19] Andersen SJ, Pikaar I, Freguia S, Lovell BC, Rabaey K, Rozendal RA. Dynamically adaptive control system for bioanodes in serially stacked bioelectrochemical systems. Environ Sci Technol 2013;47:5488–94. https://doi.org/10.1021/es400239k.
[20] Molognoni D, Bosch-Jimenez P, Suarez J, Della Pirriera M, Borràs E. How to balance the voltage in serially stacked bioelectrochemical systems. J Power Sources 2021;491. https://doi.org/10.1016/j.jpowsour.2021.229576.
[21] Rodríguez-Alegre R, Ceballos-Escalera A, Molognoni D, Bosch-Jimenez P, Galí D, Licon E, et al. Integration of membrane contactors and bio-electrochemical systems for CO2 conversion to CH4. Energies 2019;12:361. https://doi.org/10.3390/en12030361.
[22] Friis Pedersen C, Raskmark Rønne R. An efficient AC-DC electrical power converting unit configuration. 2016.
[23] Nygren L, Andrey Lana, Ahola J, Ruuskanen, Pitkänen J-P. A power converter for a bioelectrochemical system. 2021.
[24] Shahparasti M, Rocabert J, Muñoz RS, Luna A, Rodríguez P, Munoz RS, et al. Smart AC storage based on microbial electrosynthesis stack. Int Conf Renew Energy Res Appl 2018;5:1086–91. https://doi.org/10.1109/ICRERA.2018.8566904. 2018 7th.
[25] Shahparasti M, Rocabert J, Muñoz RS, Luna Pr A, Shahparasti M, Rocabert J, Muñoz RS, Luna A, Rodríguez P. Impedance source interlinking converter for microbial electrosynthesis energy storage applications. In: 2018 7th int. Conf. Renew. Energy res. Appl., vol. 5; 2018. p. 1340–5. Paris, France.
[26] Shahparasti M, Luna A, Rocabert J, Bosch P, Rodriguez P. Realization of a 10 kW MES power to methane plant based on unified AC/DC converter. Portland, OR. In: 2018 IEEE energy convers congr expo (ECCE); 2018. https://doi.org/10.1109/ECCE.2018.8558013. 3633–40.
[27] Yang H, Saeedifard M. Minimized AC circulating current for the DC – DC modular multilevel converter. IEEE Trans Ind Electron 2017;64:956–65.
[28] Freytes J, Akkari S, Rault P, Belhaouane MM, Gruson F, Colas F, et al. Dynamic analysis of MMC-based MTDC grids: use of MMC energy to improve voltage behavior. IEEE Trans Power Deliv 2019;34:137–48. https://doi.org/10.1109/TPWRD.2018.2868878.
[29] Ye H, Cao W, Chen W, Wu H, He G, Li G, et al. An AC fault ride through method for MMC-HVDC system in offshore applications including DC current-limiting inductors. IEEE Trans Power Deliv 2021:8977. https://doi.org/10.1109/TPWRD.2021.3117268.
[30] Jin Y, Xiao Q, Jia H, Mu Y, Ji Y, Teodorescu R, et al. A dual-layer back-stepping control method for lyapunov stability in modular multilevel converter based STATCOM. IEEE Trans Ind Electron 2022;69:2166–79. https://doi.org/10.1109/TIE.2021.3063973.
[31] Gontijo GF, Kerekes T, Sera D, Ricco M, Mathe L, Teodorescu R. Medium-voltage converter solution with modular multilevel structure and decentralized energy storage integration for high-power wind turbines. IEEE Trans Power Electron 2021;36:12954–67. https://doi.org/10.1109/TPEL.2021.3077501.
[32] Liang G, Tafti HD, Farivar GG, Pou J, Townsend CD, Konstantinou G. Analytical derivation of intersubmodule active power disparity limits in modular multilevel converter-based battery energy storage systems gaowen. IEEE Trans Power Electron 2021;36:594–600. https://doi.org/10.1109/ECCE44975.2020.9236261.
[33] Kumar YS, Poddar G. Balanced submodule operation of modular multilevel converter-based induction motor drive for wide-speed range. IEEE Trans Power Electron 2020;35:3918–27. https://doi.org/10.1109/TPEL.2019.2938096.
[34] Zhou S, Li B, Wang J, Xu D. A modified modular multilevel converter for motor drives capable of high-torque operation at zero/low motor speeds. IEEE Trans Circuits Syst II Express Briefs 2021;68:2493–7. https://doi.org/10.1109/TCSII.2021.3058523.

[35] Perez MA, Ceballos S, Konstantinou G, Pou J, Aguilera RP. Modular multilevel converters: recent achievements and challenges. IEEE Open J Ind Electron Soc 2021;2:224–39. https://doi.org/10.1109/ojies.2021.3060791.
[36] Pou J, Ceballos S, Konstantinou G, Agelidis VG, Picas R, Zaragoza J. Circulating current injection methods based on instantaneous information for the modular multilevel converter. IEEE Trans Ind Electron 2015;62:777–88. https://doi.org/10.1109/TIE.2014.2336608.
[37] Cheng S, Xing D, Call DF, Logan BE. Direct biological conversion of electrical current into methane by electromethanogenesis. Environ Sci Technol 2009;43:3953–8. https://doi.org/10.1021/es803531g.
[38] Cheng S, Logan BE. Sustainable and efficient biohydrogen production via electrohydrogenesis. Proc Natl Acad Sci Unit States Am 2007. https://doi.org/10.1073/pnas.0706379104.
[41] Carreon-bautista S, Erbay C, Han A, Edgar S. Power management system with integrated maximum power extraction algorithm for microbial fuel cells. IEEE Trans Energy Convers 2015;30:262–72. https://doi.org/10.1109/TEC.2014.2352654.
[42] Recio-garrido D, Perrier M, Tartakovsky B. Modeling, optimization and control of bioelectrochemical systems. Chem Eng J 2015;289:180–90. https://doi.org/10.1016/j.cej.2015.11.112.
[43] Li Z, Wang P, Chu Z, Zhu H, Luo Y, Li Y. An inner current suppressing method for modular multilevel converters. IEEE Trans Power Electron 2013;28:4873–9. https://doi.org/10.1109/TPEL.2013.2242204.
[44] Rodríguez P, Luna A, Candela I, Mujal R, Teodorescu R, Blaabjerg F. Multiresonant frequency-locked loop for grid synchronization of power converters under distorted grid conditions. IEEE Trans Ind Electron 2011;58:127–38. https://doi.org/10.1109/TIE.2010.2042420.
[45] Shahparasti M, Savaghebi M, Hosseinpour M, Rasekh N. Enhanced circular chain control for parallel operation of inverters in ups systems. Sustain Times 2020;12. https://doi.org/10.3390/su12198062.
[46] Yang S, Wang P, Tang Y, Zagrodnik MA, Hu X, King Jet T. Circulating current suppression in modular multilevel converters with even-harmonic repetitive control. IEEE Trans Ind Appl 2017;54:298–309. https://doi.org/10.1109/TIA.2017.2749257.
[47] Tu Q, Xu Z, Xu L. Reduced Switching-frequency modulation and circulating current suppression for modular multilevel converters. IEEE Trans Power Deliv 2011;26. https://doi.org/10.1109/TPWRD.2011.2115258. 2009–17.
[48] Shahparasti M, Catalan P, Garcia II, Ignacio Candela J, Tarraso A, Luna A, et al. Enhanced performance controller for high power wind converters connected to weak grids. IET Renew Power Gener 2020;14:2058–67. https://doi.org/10.1049/iet-rpg.2019.1021.